NANO LETTERS

pubs.acs.org/NanoLett Letter

Fluorinated Cyclodextrin Supramolecular Nanoassembly Enables Oxygen-Enriched and Targeted Photodynamic Therapy

Ya-Hui Song,[†] Yi-Jun Gu,[†] Zhuo Lei, Nan-Kun Li, Ying-Ming Zhang,* Qilin Yu,* and Yu Liu*

Cite This: *Nano Lett.* 2025, 25, 4476−4484 Read Online

ACCESS | Metrics & More | Article Recommendations | Supporting Information

ABSTRACT: Photodynamic therapy has become a promising treatment modality against many diseases, but its dilemma——the intrinsic hypoxia of solid tumors and the high oxygen dependence for generation of cytotoxic species——has seriously hampered its practical translation. Herein a binary supramolecular nanocarrier, which is composed of fluorocarbon chain-appended β-cyclodextrin as an oxygen carrier and adamantane-grafted hyaluronic acid as a cell-targeting agent, can deliver different types of photosensitizers by multiple noncovalent interactions. Superior to the alkylated counterpart, the fluorinated amphiphilic β-cyclodextrin can spontaneously form a nanoparticulate assembly and exhibit high oxygen-enrichment performance. The obtained nanoassembly can alleviate hypoxia in the tumor microenvironment and enhance the efficacy of photodynamic therapy. Remarkable phototoxicity and minimal dark toxicity are observed in the cancer cells, and meanwhile, preferential accumulation and significant cancer ablation are realized in the tumor-bearing mice. To be envisioned, this supramolecular assembly capable of efficiently carrying oxygen can be explored as a universal platform for precise phototherapeutics.

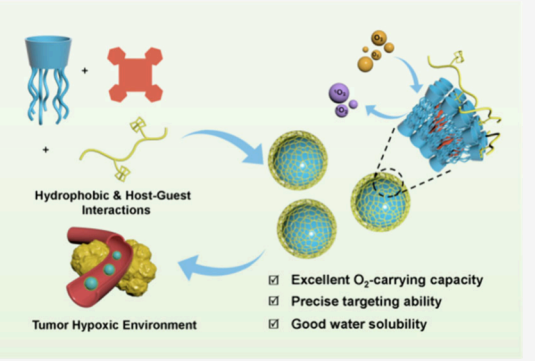

KEYWORDS: *Supramolecular theragnosis, Host−guest chemistry, Photodynamic therapy, Amphiphilic cyclodextrin assembly, Targeted drug delivery*

Photodynamic therapy (PDT), which utilizes photosensitizers (typically organic dyes), molecular oxygen (O_2), and light energy to generate reactive oxygen species (ROS), has emerged as a promising treatment modality in cancer therapeutics, mainly due to its immense advantages, such as noninvasive nature, accurate site specificity, and minimal adverse effects.[1,2] Currently, most PDT heavily relies on the supply of oxygen, leading to the abundant production of diverse ROS, including singlet oxygen ($^1O_2$), hydrogen peroxide, superoxide anion, and hydroxyl radical, via the photosensitizer-mediated energy and electron transfer processes upon light activation.[3,4] However, the naturally hypoxic tumor microenvironment, characterized by the limited oxygen levels in solid tumors arising from their dysfunctional tumor vasculature, has become a formidable challenge in the pursuit of precise and efficient PDT *in vivo*.[5−7] To overcome the hypoxia barriers in tumors, several strategies have been recently developed,[8,9] such as hypoxia-responsive photosensitizers and oxygen-generating nanoparticles.[10−13] Nevertheless, these approaches may encounter some limitations, such as heterogeneous oxygen partial pressure distribution and insufficient intratumoral ROS concentrations, which cannot sustain a prolonged oxygen supply. Meanwhile, although the oxygen-delivery efficiency has been greatly improved by the liquid perfluorocarbon-based carriers, these systems are subjected to high hydrophobicity and low surface tension and boiling point. Therefore, it is still highly imperative to improve the physicochemical performance of conventionally known photosensitizers with readily available molecular design and well understood operation mechanisms.

Multivalent supramolecular assemblies based on the cavity-bearing macrocycles, especially on cyclodextrins (CDs, a class of cyclic oligosaccharides typically possessing 6−8 D-glucose units), have been proven as an alternative or even powerful method to modulate the photophysical properties of encapsulated chromophores by leveraging the reversible and dynamic host−guest interactions.[14−19] Taking advantage of the hydrophobic cavity and hydrophilic surface of CDs, photosensitizers can be loaded in the CD's cavity to eventually achieve efficient phototheragnosis, accompanied by enhanced water solubility, sufficient ROS production, as well as controlled delivery and release via the environmentally responsive characteristics.[20−23] Therefore, it is believed that photosensitizing supramolecular entities arising from the

Received: January 6, 2025
Revised: March 5, 2025
Accepted: March 5, 2025
Published: March 8, 2025

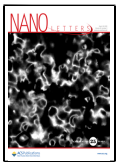

https://doi.org/10.1021/acs.nanolett.5c00090
Nano Lett. 2025, 25, 4476−4484

Scheme 1. Schematic Illustration of the Photosensitizer-Loaded HA-ADA⊂F_9CD Assembly and Its Chemical Structures

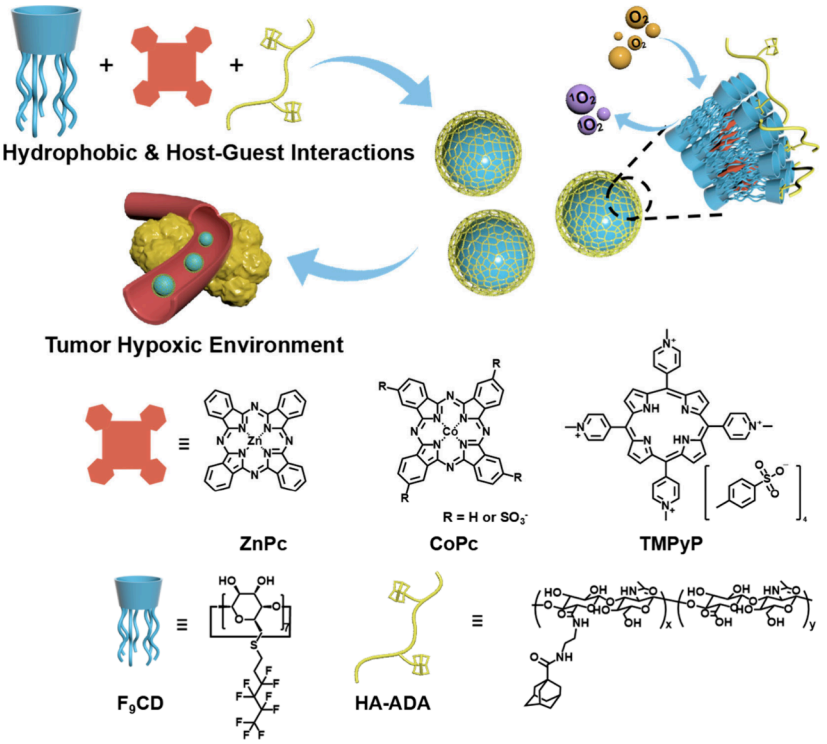

multiple host−guest interactions can offer a reliable avenue in developing PDT.[24−27] For example, Lee and Kim et al. recently reported a charge-convertible nanoparticle assembled by photosensitizer-appended β-CD and ferrocene-modified pheophorbide.[28] Under light illumination, the heptamethine cyanine dye undergoes charge conversion, thereby regulating the surface charge of nanoparticles and enabling them to maintain prolonged blood circulation for efficient penetration of tumor cells and tissue. Leveraging multivalent host−guest interactions between cyanine dyes and β-CD polymers, Yuan and Zhang et al. also developed supramolecular probes with enhanced stability, optical, and transport profiles, which can provide precise surgical navigation across various tumor models.[29] Moreover, to address the severe hypoxia in tumors, perfluorocarbons with excellent O_2-carrying capacity are commonly utilized in the PDT process.[30−32] Dai et al. designed and synthesized a porphyrin-grafted lipid that could self-assemble into nanoparticles in aqueous solution and then associate with perfluorooctyl bromide for substantial enhancement of PDT efficacy.[33] Nevertheless, the construction of universal photosensitizer-compatible nanoplatforms that can effectively deliver oxygen and target tumor tissues has rarely been reported by utilizing multiple noncovalent interactions.

In this study, we report a supramolecular nanocarrier based on the multivalent interactions between fluorinated β-CD and adamantylated hyaluronic acid, which can achieve the targeted delivery of different types of photosensitizers with high O_2-carrying capacity (Scheme 1). By virtue of the extensive hydrophobic region of fluorocarbon chains, photosensitizers can be readily loaded as cargos while maintaining high loading contents of oxygen. More remarkably, after equipment with the adamantane-modified hyaluronic acid through multiple host−guest interactions, a secondary nanoparticulate assembly is formed to facilitate its targeted internalization in cancer cells. The *in vivo* examination using tumor-bearing mice models further demonstrates that efficient cancer ablation could be achieved by such amphiphilic fluorinated β-CD assembly with an enhanced PDT therapeutic efficacy. To be envisioned, this oxygen self-enriched supramolecular assembly featuring high biocompatibility, exceptional photosensitizing activity, and compelling cell/tissue selectivity can be exploited as a universal nanoplatform for targeted delivery of photosensitizers and may hold great promise for PDT applications under hypoxia.

The amphiphilic β-CD derivatives appended with seven fluoroalkyl thiols at the primary face were synthesized through the nucleophilic substitution reaction with heptakis(6-iodo-6-deoxy)-β-CD under strong basic condition. To achieve the balance between the O_2 solubility of fluorocarbon chains and the amphiphilicity of the whole molecule, the one bearing 2-(perfluorobutyl)ethanethiol substituents (F_9CD) was selected (Scheme S1 and Figures S1−S3, Supporting Information), allowing the high-content fluorocarbon chains for O_2-carrying capacity and satisfactory water solubility at the same time. For a comparative purpose, the reference compound with only the hydrocarbon alkyl chain (H_9CD) was also synthesized in a moderate yield (Scheme S2 and Figures S4−S5, Supporting Information). Meanwhile, three typical photosensitizers, including neutral ZnPc, positively charged TMPyP, and negatively charged CoPc,[34,35] were chosen for the study of F_9CD-improved PDT performance.

Due to its amphiphilic property, F_9CD was prone to self-aggregation into nanoparticles in aqueous solution. The critical aggregation concentration (CAC) of F_9CD was determined by monitoring its UV−vis transmittance at various concentrations. As shown in Figure 1a, the transmittance at 500 nm exhibited an inflection point at 15 μM as the concentration increased, corresponding to the identification of the CAC value and the transition of F_9CD from monomers to self-assembled nanoparticles (Figure 1a).

https://doi.org/10.1021/acs.nanolett.5c00090
Nano Lett. 2025, 25, 4476−4484

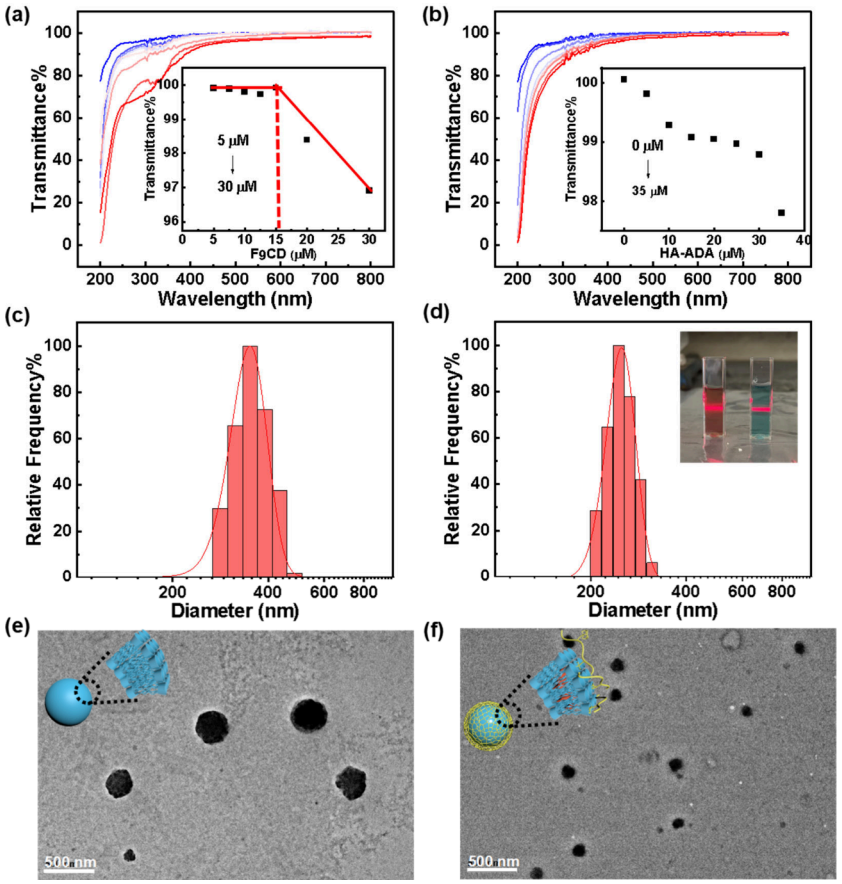

Figure 1. (a) Optical transmittance of F_9CD at different concentrations; Inset: optical transmittance changes of F_9CD at 500 nm versus concentrations ([F_9CD] = 5−30 μM). (b) Optical transmittance of F_9CD with different concentrations of HA-ADA; Inset: optical transmittance changes of F_9CD at 500 nm versus concentrations of HA-ADA ([F_9CD] = 10 μM and [HA-ADA] = 0−35 μM). DLS profiles of (c) F_9CD and (d) TMPyP@HA-ADA⊂F_9CD. Inset: The corresponding Tyndall effects of (right) TMPyP@HA-ADA⊂F_9CD and (left) CoPc@HA-ADA⊂F_9CD assemblies in aqueous solution. TEM images of (e) F_9CD and (f) TMPyP@HA-ADA⊂F_9CD.

It is known that hyaluronic acid (HA) can specifically recognize the surface of cancer cells via the receptor-mediated endocytosis.[36,37] In our case, the addition of adamantane-modified hyaluronic acid (HA-ADA) could not only endow the resultant F_9CD amphiphile with desired cell-targeting ability but also provide new possibilities to further adjust the amphiphilicity and induce the secondary coassembly through the strong host−guest complexation between β-CD and ADA moieties (Scheme S3 and Figure S6, Supporting Information). Using a 10 μM F_9CD solution (below its CAC value), the obtained transmittance continuously decreased upon gradual addition of HA-ADA (Figure 1b). It is speculated that the addition of HA-ADA could induce the formation of nano-aggregation with F_9CD in solution and, thus, lower the CAC value of this binary system. In addition, the Zeta potential measurements showed that the HA-ADA⊂F_9CD nanoparticles gave a negative charge distribution on the surface (ζ = −42.3 eV), while this value slightly varied in the presence of different photosensitizers (Figure S7, Supporting Information).

The hydrodynamic diameters of the nanoparticles were measured by dynamic light scattering (DLS) experiments, and the average value for F_9CD alone was obtained as 351 nm in solution (Figure 1c). Meanwhile, the Tyndall effect was clearly observed in the cases of TMPyP- and CoPc-loaded HA-ADA⊂F_9CD assemblies, once again confirming the formation of large-sized secondary nanoaggregates in the aqueous phase. The DLS data also found that the obtained nanoparticulate assembly remained stable for at least 7 days (Figure S8, Supporting Information). Notably, compared to free F_9CD nanoaggregates, the incorporation of HA-ADA resulted in a significant reduction in the hydrodynamic diameters of the nanoparticles from 351 to 201 nm (Figure 1c and 1d). This phenomenon may contribute to the intermolecular cross-linking of F_9CD amphiphiles by HA-ADA, which would lead to the formation of more compact assembled structures and eventually facilitate better penetration into tumor sites. Accordingly, the morphological characterization in the solid state was also conducted by transmission electron microscopy (TEM), and the assembly sizes of free and photosensitizer-loaded F_9CD amphiphiles were measured as 220 and 120 nm, respectively, which were basically consistent with the DLS results (Figure 1e and 1f).

The O_2 enrichment performance of F_9CD relative to pure water was comparatively evaluated using H_9CD as the reference compound. Benefiting from the excellent O_2-dissolving capacity of fluorocarbon segments,[33,38] the O_2 molecules could be easily entrapped by the hydrophobic region of F_9CD. After addition of a large amount of deoxygenated water (pretreatment with N_2) into the O_2-saturated HA-ADA⊂F_9CD, HA-ADA⊂H_9CD, and pure water as control, respectively, the changes of O_2 concentration in solution were monitored by a dissolved oxygen portable meter.

https://doi.org/10.1021/acs.nanolett.5c00090
Nano Lett. 2025, 25, 4476−4484

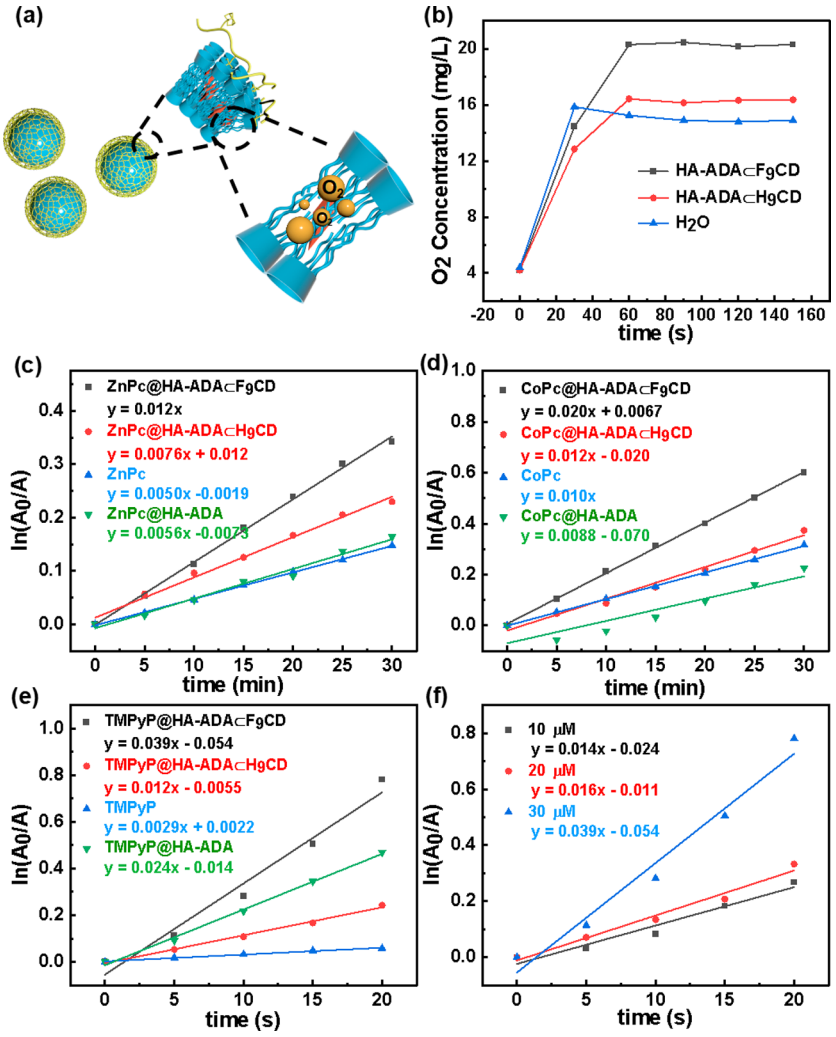

Figure 2. (a) Schematic diagram of transport of O_2 by the obtained assembly. (b) Changes in the concentration of O_2 versus time after addition of HA-ADA⊂F_9CD and HA-ADA⊂H_9CD into deoxygenated water ([F_9CD] = [H_9CD] = 100 μM and [HA-ADA] = 100 μM). Decomposition rates of ABDA at 378 nm versus irradiation time by (c) ZnPc@HA-ADA⊂F_9CD, (d) CoPc@HA-ADA⊂F_9CD, (e) TMPyP@HA-ADA⊂F_9CD ([photosensitizer] = [F_9CD] = [H_9CD] = [HA-ADA] = 30 μM, [ABDA] = 150 μM), and (f) TMPyP@HA-ADA⊂F_9CD at different carrier concentrations ([TMPyP] = 30 μM, [ABDA] = 150 μM).

As shown in Figure 2b, the F_9CD solution gave the maximum releasing amount of 20.3 mg/L in 150 s. Though H_9CD possesses a certain O_2-carrying ability by its hydrophobic alkyl chains, the releasing amount was significantly lower than that of the fluoroalkylated β-CD over the same time interval. These results jointly corroborated that the HA-ADA⊂F_9CD assembly could readily release the entrapped O_2 in the tumor hypoxic microenvironments, which may facilitate the successful implementation of PDT in tumor tissue, as described below.

Initially, ZnPc was utilized to quantitatively assess the enhancement effect of a supramolecular amphiphilic system on the $^1O_2$ generation yields ($\phi\Delta$) of various photosensitizers (Figure S9, Supporting Information). As discerned from Figure 2c, the incorporation of ZnPc into the HA-ADA⊂F_9CD assembly led to a marked increase in the $\phi\Delta$ value, which was 2.4-fold higher than that of ZnPc alone. In the control experiment, no obvious enhancement effect was found by the free HA-ADA, thereby validating the important role of the F_9CD amphiphilic assembly in improving the photosensitizing performance.

To further substantiate the versatility of our delivery system, the scope of photosensitizers was extended to positively charged porphyrin (TMPyP) and negatively charged phthalocyanine (CoPc). As can be seen from Table S1 (Supporting Information), the HA-ADA⊂F_9CD assembly exhibited significant $^1O_2$ enhancement for all the distinct photosensitizers (Figures S10 and S11, Supporting Information). The most pronounced effect was achieved in the case of TMPyP, where the $\phi\Delta$ value of the TMPyP@HA-ADA⊂F_9CD assembly surpassed that of free TMPyP by a remarkable factor of 13.3. In addition, the control experiment demonstrated that the presence of HA-ADA increases singlet oxygen production by 8.1 times as compared to free TMPyP, which is mainly attributed to the suppression of undesired self-aggregation of photosensitizers by the electrostatic attraction with the HA chain (Figure 2e). In addition, the host−guest complexation between F_9CD and ADA could draw the photosensitizer and the O_2-rich fluorocarbon chains much closer, ultimately fostering a synergistic effect to amplify the $^1O_2$ yield of the TMPyP@ HA-ADA⊂F_9CD assembly. In contrast, the electrostatic repulsion is an unfavorable driving force in the case of

https://doi.org/10.1021/acs.nanolett.5c00090
Nano Lett. 2025, 25, 4476−4484

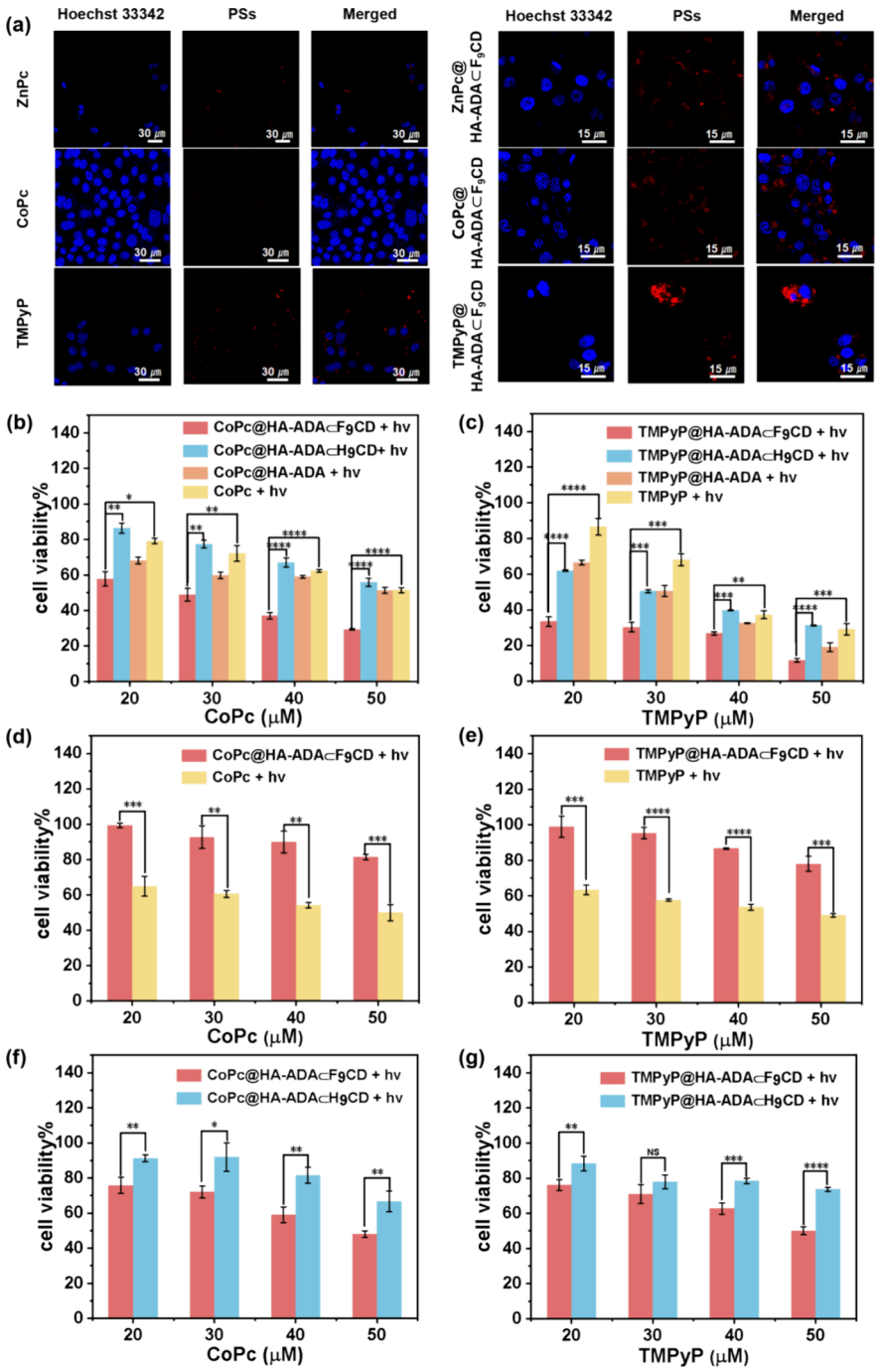

Figure 3. *In vitro* evaluation of the anticancer activity of the assemblies. (a) CLSM images of living A549 cells treated with ZnPc, CoPc, TMPyP, ZnPc@HA-ADA⊂F_9CD, CoPc@HA-ADA⊂H_9CD, and TMPyP@HA-ADA⊂H_9CD assemblies, respectively. [photosensitizer] = 10 μM, [F_9CD] = 10 μM, and [HA-ADA] = 10 μM. Cell nuclei were stained with Hoechst 33342. The scale bar is 30 or 15 μm. Phototoxicity of (b) CoPc- and (c) TMPyP-involved assemblies in A549 cells. Comparison of phototoxicity of (d) CoPc@HA-ADA⊂F_9CD and (e) TMPyP@HA-ADA⊂F_9CD with individual photosensitizers in 293T cells. Comparison of photocytotoxicity of (f) CoPc@HA-ADA⊂F_9CD and (g) TMPyP@HA-ADA⊂F_9CD with their H_9CD-involved reference assembly in A549 cells under hypoxic condition. Statistical analysis of the data was carried out by independent-samples' *t* test and data presented are the means ± standard error of the mean (S.E.M.) (n = 3). *p < 0.05, **p < 0.01, ***p < 0.001, and ****p < 0.0001.

CoPc@HA-ADA and resulted in the lowest the $\phi\Delta$ value among all the CoPc-involved groups (Figure 2d). Moreover, the loading capacity and encapsulation efficiency of three photosensitizers have been calculated as 4.02% and 29.1%, 6.1% and 34.0%, as well as 14.8% and 64.2%, for ZnPc-, CoPc-, and TMPyP-loaded F_9CD⊂HA-ADA nanoassemblies, respectively (Figure S12, Supporting Information).

It is also found that the $^1O_2$ generation rate of the TMPyP-loaded assemblies was in proportion to the HA-ADA⊂F_9CD concentration when the concentration of photosensitizer was fixed at 30 μM, further corroborating the large O_2-loading capacity of the fluorinated supramolecular carrier (Figures 2f and S13, Supporting Information). In comparison, the TMPyP@HA-ADA⊂H_9CD assembly gave a lower $\phi\Delta$ value

https://doi.org/10.1021/acs.nanolett.5c00090
Nano Lett. 2025, 25, 4476−4484

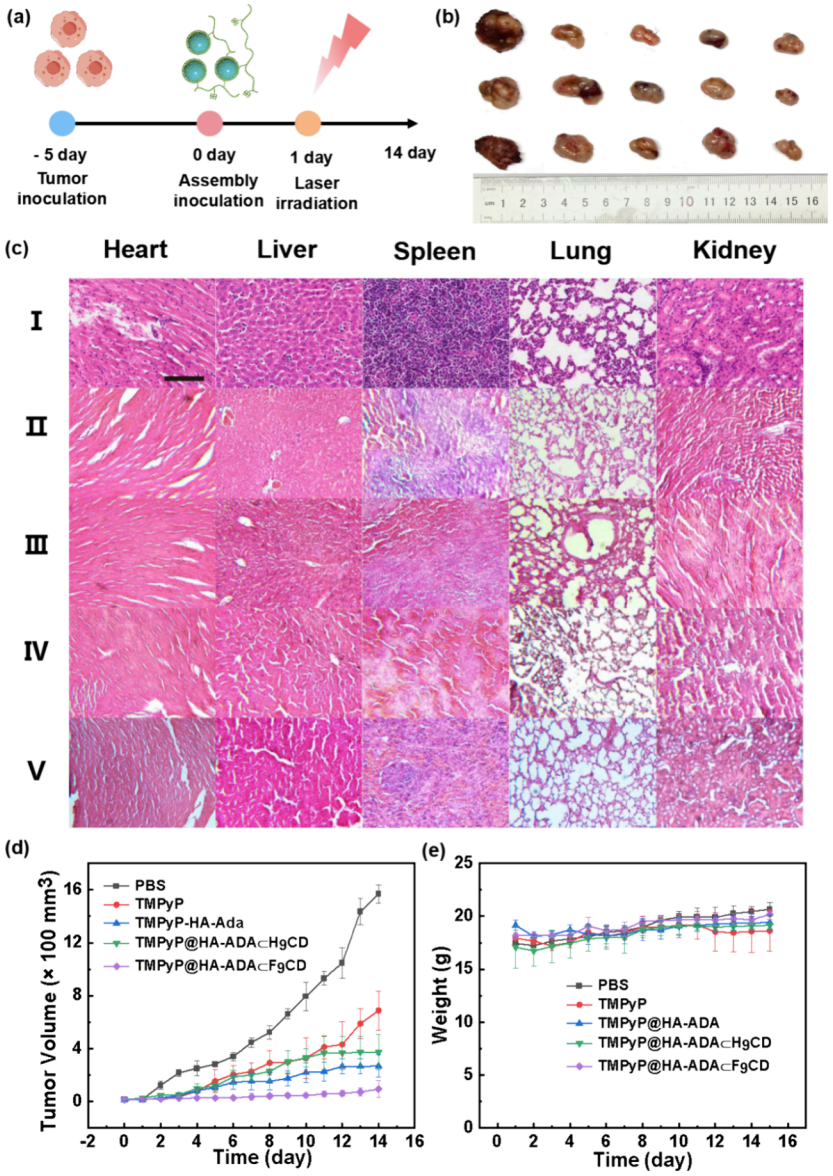

Figure 4. *In vivo* evaluation of the PDT efficacy of the assemblies of TMPyP under light irradiation (220 mW/cm^2). (a) Schematic illustration of the establishment of the tumor model in mice and the tail vein injection of the drug. (b) Representative photographs of tumors of the tumor-bearing mice in different groups on the 14th day. (I: PBS; II: TMPyP; III: TMPyP@HA-ADA; IV: TMPyP@HA-ADA⊂H_9CD; V: TMPyP@HA-ADA⊂F_9CD) (c) H&E staining of tumor tissues from different samples of tumor-bearing mice. The scale bars are 200 μm. Body weights (d) and tumor volumes (e) of the mice in different groups during 14 days of treatment.

than that of its fluorocarbon-based counterparts or even the TMPyP@HA-ADA group. This finding could be attributed to the partial aggregation of photosensitizers within the hydrophobic domains of the TMPyP@HA-ADA⊂H_9CD nanoparticles. However, the O_2-carrying capacity of the alkyl chains in H_9CD is significantly inferior to that of the fluorocarbon chains in F_9CD, and consequently, the reduced accessibility to O_2 in the alkyl chain environment may largely hinder the efficient $^1O_2$ generation in the TMPyP@HA-ADA⊂H_9CD assembly.

To further demonstrate the cellular uptake behaviors, confocal laser scanning microscopy (CLSM) imaging experiments were performed. After coincubation with A549 cells for 24 h, the red-fluorescence dots arising from the photosensitizers were clearly observed and uniformly scattered in cytoplasm in the presence of F_9CD and HA-ADA, whereas weaker fluorescence was observed by free photosensitizers (Figure 3a and S14, Supporting Information). This result indicates that the photosensitizer-embedded HA-ADA⊂F_9CD assemblies could be easily internalized and accumulated in the cells. Next, the cytotoxicity of different samples was evaluated using the standard cell counting Kit-8 (CCK-8) assay under different conditions. Initially, the dark cytotoxicity of free carriers and the photosensitizer-loaded assemblies was tested. As shown in Figure S15 (Supporting Information), the cell viability remained above 90% for both normal (293T) and tumor cells (A549) after incubation for 24 h, suggesting their good biocompatibility and biosafety without light irradiation.

The phototoxicity of A549 cells was assessed upon light exposure under normal oxygen condition (Figure 3b and 3c), and the half maximal inhibitory concentrations (IC_{50}) are tabulated in Table S2 (Supporting Information). The cell viability in the CoPc@HA-ADA⊂F_9CD group (CoPc for 50 μM) was dramatically reduced to only 29% upon light

https://doi.org/10.1021/acs.nanolett.5c00090
Nano Lett. 2025, 25, 4476−4484

irradiation for 15 min, while these values were measured as 56% and 51% for the CoPc@HA-ADA⊂H_9CD and CoPc@HA-ADA groups, respectively. It is noted that although the singlet oxygen generated by CoPc@HA-ADA is 2-fold higher than that generated by CoPc@HA-ADA⊂H_9CD, they showed very similar IC_{50} values in A549 cells. In our case, CoPc@HA-ADA⊂H_9CD was presented as a uniform nanoparticulate assembly, whereas CoPc@HA-ADA only gave an amorphous aggregate (Figure S16, Supporting Information). The formation of the nanoparticulate assembly is favorable for cell uptake and can compensate for the inferiority in $^1O_2$ generation to some extent, thus leading to no significant cytotoxicity differences between CoPc@HA-ADA and CoPc@HA-ADA⊂H_9CD assemblies. Moreover, when TMPyP served as a photosensitizer, TMPyP@HA-ADA⊂F_9CD exhibited superior phototoxicity with the cell viability of 11%, while TMPyP@HA-ADA⊂H_9CD and TMPyP alone could only decrease the cell viability to 32% and 29%, respectively. Notably, the difference in cell viability became more significant at a much lower concentration of photosensitizers. Taking TMPyP at 20 μM as an example, the presence of HA-ADA⊂F_9CD could greatly decrease the cell viability to 33%, compared to 66% and 86% for TMPyP@HA-ADA⊂H_9CD and TMPyP@HA-ADA, respectively. More remarkably, benefiting from the existence of HA-ADA as the cell-targeting agent, the resultant assemblies could easily distinguish the malignant cells from the normal ones, thereby leading to the large distinction in A549 cell and 293T cell viability (i.e., 29% vs 81% in the CoPc-involved group and 11% vs 78% in the TMPyP-involved group, respectively, at 50 μM photosensitizers) (Figure 3d and 3e).

Subsequently, the *in vitro* anticancer activities were also comparatively studied under hypoxic condition (1.1% O_2). Analogous to the results under normoxic conditions, the involvement of HA-ADA⊂F_9CD could induce cell death more markedly than HA-ADA⊂H_9CD after loading photosensitizers under hypoxia condition. Also, it is noted that the whole cell viability was marginally elevated under hypoxic compared to normoxic conditions (Figure 3f and 3g). Apparently, this result is mainly attributed to the inadequate supply of intracellular ROS under hypoxic condition. Nevertheless, due to its superior O_2-enriching capability, the HA-ADA⊂F_9CD carrier would effectively mitigate the decline in PDT efficacy caused by hypoxia in the tumor microenvironment. In addition, the ROS production in the cell environment was assessed using 6-carboxy- 2′,7′-dichlorodihydrofluorescein diacetate (DCFH-DA) as a fluorescent indicator. As shown in Figure S17 (Supporting Information), compared to other control groups, the brightest green fluorescence was exclusively observed in the A549 cells, implying that a large amount of ROS could be produced with a high quantum yield by the TMPyP@HA-ADA⊂F_9CD assembly after light irradiation.

Enthusiastic about these findings in an inanimate milieu and cancer cells, the *in vivo* therapeutic efficacy was further investigated using the tumor-bearing mouse model. In this case, TMPyP was chosen as the ideal photosensitizer on account of its extremely high loading efficiency by the HA-ADA⊂F_9CD carrier. First, to evaluate the tumor-targeting efficacy of TMPyP@HA-ADA⊂F_9CD nanoparticles, systemic administration studies were conducted in tumor-bearing mice (Figure S18, Supporting Information). The *ex vivo* fluorescence images reveals that the red-fluorescence nanoassemblies were predominantly accumulated in tumor tissues, accompanied by weak signals detected in the hepatic clearance organs. This biodistribution pattern demonstrates the significant tumor-targeting specificity of the obtained nanoconstructs. Next, the TMPyP-loaded supramolecular amphiphiles and the corresponding control groups were administered to the mice via tail vein injection, and the tumor sites were irradiated by white light after incubation in the dark for 24 h (Figure 4a). The tumor volumes and body weights of the mice were meticulously recorded over a period of 14 days (Figure 4b and 4c). Although the body weights remained basically unchanged in all of the examined groups, the TMPyP@HA-ADA⊂F_9CD group showed the best inhibition effect with statistically significant differences. The tumor growth inhibition rate was calculated up to 94%, which exceeded its counterpart formulations, including TMPyP@HA-ADA⊂H_9CD (76%), TMPyP@HA-ADA (82%), and free TMPyP (56%, Figure 4d). Collectively, these findings underscore the potent antitumor activity of the TMPyP@HA-ADA⊂F_9CD nanoassembly, which may hold great promise as a therapeutic agent.

Upon completion of the *in vivo* experiment, the tumor-bearing mice were euthanized, and subsequent hematoxylin and eosin (H&E) staining of crucial organs and tumor tissues was conducted. As can be seen from Figure 4e, superior to other control groups, no discernible tissue damage or pathological alteration was observed after administration of TMPyP@HA-ADA⊂F_9CD, thus highlighting the exceptional biocompatibility and biosafety profile of the supramolecular photodynamic therapies.

In conclusion, to overcome the obstacles in the current PDT, amphiphilic F_9CD was synthesized and exploited as a versatile supramolecular nanocarrier by harnessing the O_2-enriched ability of perfluorocarbon chains and the encapsulating ability of CD's cavity. The fluoroalkylated tails in F_9CD can dissolve O_2 molecules and load diverse photosensitizing cargos via the hydrophobic interaction, and the β-CD's cavity can coassemble with the cell-targeting agent HA-ADA via host−guest complexation. In an inanimate milieu, spectroscopic study revealed that the $^1O_2$ production yield was dramatically augmented in aqueous solution by substantially mitigating the intermolecular self-aggregation of photosensitizers. At the cellular level, the photosensitizer-equipped supramolecular amphiphiles exhibited pronounced phototoxicity exclusively toward cancer cells and could not make any negative impact on cell viability in the dark. In the murine mode, the representative TMPyP@HA-ADA⊂F_9CD ternary assembly could ablate tumors associated with minimal systemic toxicity at therapeutically relevant concentrations. Given good targetability, biocompatibility, and versatility, it can be envisioned that our work is easily amenable to many different photosensitive drugs and may be developed as a universal approach against cancers and other diseases in a cost-effective manner.

■ ASSOCIATED CONTENT

Supporting Information

The Supporting Information is available free of charge at https://pubs.acs.org/doi/10.1021/acs.nanolett.5c00090.

Synthesis schemes (S1−S3), NMR and MALDI-TOF spectra (Figures S1−S6), Zeta potentials (Figure S7), stability evaluation of nanoparticles (Figure S8), UV−vis spectra (Figures S9−S11, S13), loading capacity and encapsulation efficiency of photosensitizers (Figure

https://doi.org/10.1021/acs.nanolett.5c00090
Nano Lett. 2025, 25, 4476−4484

S12), fluorescence emission spectra of nanoparticulate assemblies (Figure S14), dark cytotoxicity (Figure S15), TEM images (Figure S16), cell culture and animal breeding, CLSM images of DCFH-DA (Figure S17), *ex vivo* distribution of TMPyP@HA-ADA⊂F_9CD (Figure S18). (PDF)

AUTHOR INFORMATION

Corresponding Authors

Ying-Ming Zhang − *College of Chemistry, State Key Laboratory of Elemento-Organic Chemistry, Collaborative Innovation Center of Chemical Science and Engineering (Tianjin), Nankai University, Tianjin 300071, P. R. China*; Email: ymzhang@nankai.edu.cn

Qilin Yu − *Key Laboratory of Molecular Microbiology and Technology, Ministry of Education, Department of Microbiology, College of Life Sciences, Nankai University, Tianjin 300071, China*; orcid.org/0000-0003-0473-5111; Email: yuqilin@mail.nankai.edu.cn

Yu Liu − *College of Chemistry, State Key Laboratory of Elemento-Organic Chemistry, Collaborative Innovation Center of Chemical Science and Engineering (Tianjin), Nankai University, Tianjin 300071, P. R. China*; orcid.org/0000-0001-8723-1896; Email: yuliu@nankai.edu.cn

Authors

Ya-Hui Song − *College of Chemistry, State Key Laboratory of Elemento-Organic Chemistry, Collaborative Innovation Center of Chemical Science and Engineering (Tianjin), Nankai University, Tianjin 300071, P. R. China*

Yi-Jun Gu − *Key Laboratory of Molecular Microbiology and Technology, Ministry of Education, Department of Microbiology, College of Life Sciences, Nankai University, Tianjin 300071, China*

Zhuo Lei − *College of Chemistry, State Key Laboratory of Elemento-Organic Chemistry, Collaborative Innovation Center of Chemical Science and Engineering (Tianjin), Nankai University, Tianjin 300071, P. R. China*; orcid.org/0000-0001-6042-6810

Nan-Kun Li − *College of Chemistry, State Key Laboratory of Elemento-Organic Chemistry, Collaborative Innovation Center of Chemical Science and Engineering (Tianjin), Nankai University, Tianjin 300071, P. R. China*

Complete contact information is available at: https://pubs.acs.org/10.1021/acs.nanolett.5c00090

Author Contributions

†Y.-H.S. and Y.-J.G. contributed equally to this work.

Notes

The authors declare no competing financial interest.

ACKNOWLEDGMENTS

This work was financially supported by National Natural Science Foundation of China (22171148, 22371148, and 22131008), Haihe Laboratory of Sustainable Chemical Transformation, and the Fundamental Research Funds for the Central Universities (Nankai University).

REFERENCES

(1) Yang, B.; Chen, Y.; Shi, J. Reactive Oxygen Species (ROS)-Based Nanomedicine. *Chem. Rev.* **2019**, *119*, 4881.

(2) Dolmans, D. E.; Fukumura, D.; Jain, R. K. Photodynamic Therapy for Cancer. *Nat. Rev. Cancer* **2003**, *3*, 380−387.

(3) Agostinis, P.; Berg, K.; Cengel, K. A.; Foster, T. H.; Girotti, A. W.; Gollnick, S. O.; Hahn, S. M.; Hamblin, M. R.; Juzeniene, A.; Kessel, D.; et al. Photodynamic Therapy of Cancer: An Update. *CA Cancer J. Clin.* **2011**, *61*, 250−281.

(4) Celli, J. P.; Spring, B. Q.; Rizvi, I.; Evans, C. L.; Samkoe, K. S.; Verma, S.; Pogue, B. W.; Hasan, T. Imaging and Photodynamic Therapy: Mechanisms, Monitoring, and Optimization. *Chem. Rev.* **2010**, *110*, 2795−2838.

(5) Qi, G.; Hu, F.; Kenry; Shi, L.; Wu, M.; Liu, B. An AIEgen-Peptide Conjugate as a Phototheranostic Agent for Phagosome Entrapped Bacteria. *Angew. Chem., Int. Ed.* **2019**, *58*, 16229.

(6) Yao, C.; Wang, W.; Wang, P.; Zhao, M.; Li, X.; Zhang, F. Near-Infrared Upconversion Mesoporous Cerium Oxide Hollow Biophotocatalyst for Concurrent pH-/H_2O_2-Responsive O_2-Evolving Synergetic Cancer Therapy. *Adv. Mater.* **2018**, *30*, No. 1704833.

(7) Wang, H.; Han, X.; Dong, Z.; Xu, J.; Wang, J.; Liu, Z. Hyaluronidase with pH Responsive Dextran Modification as an Adjuvant Nanomedicine for Enhanced Photodynamic Immunotherapy of Cancer. *Adv. Funct. Mater.* **2019**, *29*, No. 1902440.

(8) Chen, X.; Mendes, B. B.; Zhuang, Y.; Conniot, J.; Mercado Argandona, S.; Melle, F.; Sousa, D. P.; Perl, D.; Chivu, A.; Patra, H. K.; Shepard, W.; Conde, J.; Fairen-Jimenez, D. A Fluorinated BODIPY-Based Zirconium Metal−Organic Framework for In Vivo Enhanced Photodynamic Therapy. *J. Am. Chem. Soc.* **2024**, *146*, 1644−1656.

(9) Zhao, J.; Yang, Y.; Xu, X.; Li, H.; Fei, J.; Liu, Y.; Zhang, X.; Li, J. Super Light-Sensitive Photosensitizer Nanoparticles for Improved Photodynamic Therapy against Solid Tumors. *Angew. Chem., Int. Ed.* **2022**, *61*, No. e202210920.

(10) Fan, Z.; Teng, K.-X.; Xu, Y.-Y.; Niu, L.-Y.; Yang, Q.-Z. The Photodynamic Agent Designed by Involvement of Hydrogen Atom Transfer for Enhancing Photodynamic Therapy. *Angew. Chem., Int. Ed.* **2025**, *64*, No. e20241359.

(11) Teng, K.-X.; Zhang, D.; Liu, B.-K.; Liu, Z.-F.; Niu, L.-Y.; Yang, Q.-Z. Photo-Induced Disproportionation-Mediated Photodynamic Therapy: Simultaneous Oxidation of Tetrahydrobiopterin and Generation of Superoxide Radicals. *Angew. Chem., Int. Ed.* **2024**, *63*, No. e20231878.

(12) Xiong, T.; Peng, Q.; Chen, Y.; Li, M.; Du, J.; Fan, J.; Jia, L.; Peng, X. A Novel Nanobody-Photosensitizer Conjugate for Hypoxia Resistant Photoimmunotherapy. *Adv. Funct. Mater.* **2021**, *31*, No. 2103629.

(13) Li, M.; Xu, Y.; Xiong, T.; Huang, H.; Long, S.; Yu, L.; Singh, N.; Tong, Y.; Sessler, J. L.; Peng, X.; Kim, J. S. Photoredox Catalysis May be a General Mechanism in Photodynamic Therapy. *Proc. Natl. Acad. Sci. U. S. A.* **2022**, *119*, No. e2210504119.

(14) Liu, Z.; Dai, X.; Sun, Y.; Liu, Y. Organic Supramolecular Aggregates Based on Water-Soluble Cyclodextrins and Calixarenes. *Aggregate* **2020**, *1*, 31−44.

(15) Liu, Z.; Lin, W.; Liu, Y. Macrocyclic Supramolecular Assemblies Based on Hyaluronic Acid and Their Biological Applications. *Acc. Chem. Res.* **2022**, *55*, 3417−3429.

(16) Liu, Z.; Liu, Y. Multicharged Cyclodextrin Supramolecular Assemblies. *Chem. Soc. Rev.* **2022**, *51*, 4786−4827.

(17) Zhang, Y.-M.; Liu, Y.-H.; Liu, Y. Cyclodextrin-Based Multistimuli-Responsive Supramolecular Assemblies and Their Biological Functions. *Adv. Mater.* **2019**, *3*, No. 1806158.

(18) He, S.; Wang, L.; Wu, D.; Tong, F.; Zhao, H.; Li, H.; Gong, T.; Gao, H.; Zhou, Y. Dual-responsive Supramolecular Photodynamic Nanomedicine with Activatable Immunomodulation for Enhanced Antitumor Therapy. *Acta Pharm. Sin B* **2024**, *14*, 765−780.

(19) Yin, Y.; Sun, P.; Dong, H.; Chen, Y.; Chen, S.; Wang, L. Supramolecular Nanoparticles Constructed by Orthogonal Assembly of Pillar[5]arene-Cyclodextrin Dimacrocycle for Chemo-Photodynamic Combination Therapy. *Chin. Chem. Lett.* **2023**, *34*, No. 108594.

(20) Wang, W.; Tham, P. H.; Ding, C.; Huang, P.; Li, T.; Luo, J.; Xiang, H.; Zeng, X.; Chen, H.; Zhao, Y. Transethosome-Based

Topical Administration Systems with Enhanced Penetration and Dual Actions for Treating EGFR-Overexpressed Cutaneous Squamous Cell Carcinoma. *Adv. Funct. Mater.* **2024**, *34*, No. 2312838.
(21) Xu, M.; Zha, H.; Han, R.; Cheng, Y.; Chen, J.; Yue, L.; Wang, R.; Zheng, Y. Cyclodextrin-Derived ROS-Generating Nanomedicine with pH-Modulated Degradability to Enhance Tumor Ferroptosis Therapy and Chemotherapy. *Small* **2022**, *18*, No. 2200330.
(22) Sarkar, S.; Chatterjee, A.; Kim, D.; Saritha, C.; Barman, S.; Jana, B.; Ryu, J. H.; Das, A. Host-Guest Adduct as a Stimuli-Responsive Prodrug: Enzyme-Triggered Self-Assembly Process of a Short Peptide within Mitochondria to Induce Cell Apoptosis. *Adv. Healthc. Mater.* **2025**, *14*, No. 2403243.
(23) Meng, L.-B.; Zhang, W.; Li, D.; Li, Y.; Hu, X.-Y.; Wang, L.; Li, G. pH-Responsive Supramolecular Vesicles Assembled by Water-Soluble Pillar[5]arene and a BODIPY Photosensitizer for Chemo-Photodynamic Dual Therapy. *Chem. Commun.* **2015**, *51*, 14381−14384.
(24) Yuan, X.; Xu, D.-F.; Song, Y.-H.; Zhang, Y.-M.; Liu, Y. Cucurbituril-Based Porphyrin Cascade Assembly for Cell Imaging and Targeted Drug Delivery. *ACS Appl. Polym. Mater.* **2024**, *6*, 4331−4338.
(25) Dai, X.; Huo, M.; Zhang, B.; Liu, Z.; Liu, Y. Folic Acid-Modified Cyclodextrin Multivalent Supramolecular Assembly for Photodynamic Therapy. *Biomacromolecules* **2022**, *23*, 3549−3559.
(26) Tang, M.; Liu, Y.-H.; Liu, H.; Mao, Q.; Yu, Q.; Hiroaki, K. Supramolecular Dual Polypeptides Induced Tubulin Aggregation for Synergistic Cancer Theranostics. *J. Med. Chem.* **2022**, *65*, 13473−13481.
(27) Hou, D.-Y.; Cheng, D.-B.; Zhang, N.-Y.; Wang, Z.-J.; Hu, X.-J.; Lv, M.-Y.; Li, X.-P.; Jian, L.-R.; Ma, J.-P.; Sun, T.; Qiao, Z.-Y.; Xu, W.; Wang, H. In Vivo Assembly Enhanced Binding Effect Augments Tumor Specific Ferroptosis Therapy. *Nat. Commun.* **2024**, *15*, 454.
(28) Nguyen, D.-T.; Baek, M.-J.; Lee, S.; Kim, D.; Yoo, S.-Y.; Lee, J.-Y.; Kim, D.-D. Photobleaching-Mediated Charge-Convertible Cyclodextrin Nanoparticles Achieve Deep Tumour Penetration for Rectal Cancer Theranostics. *Nat. Nanotechnol.* **2024**, *19*, 1723−1734.
(29) Wu, Q.; Zhou, Z.; Xu, L.; Zhong, H.; Xiong, B.; Ren, T.; Li, Z.; Yuan, L.; Zhang, X.-B. Multivalent Supramolecular Fluorescent Probes for Accurate Disease Imaging. *Sci. Adv.* **2024**, *10*, No. eadp8719.
(30) Ren, H.; Liu, J.; Su, F.; Ge, S.; Yuan, A.; Dai, W.; Wu, J.; Hu, Y. Relighting Photosensitizers by Synergistic Integration of Albumin and Perfluorocarbon for Enhanced Photodynamic Therapy. *ACS Appl. Mater. Interfaces* **2017**, *9*, 3463−3473.
(31) Que, Y.; Liu, Y.; Tan, W.; Feng, C.; Shi, P.; Li, Y.; Huang, X. Enhancing Photodynamic Therapy Efficacy by Using Fluorinated Nanoplatform. *ACS Macro Lett.* **2016**, *5*, 168−173.
(32) Song, G.; Liang, C.; Yi, X.; Zhao, Q.; Cheng, L.; Yang, K.; Liu, Z. Perfluorocarbon-Loaded Hollow Bi_2Se_3 Nanoparticles for Timely Supply of Oxygen under Near-Infrared Light to Enhance the Radiotherapy of Cancer. *Adv. Mater.* **2016**, *28*, 2716−2723.
(33) Liang, X.; Chen, M.; Bhattarai, P.; Hameed, S.; Dai, Z. Perfluorocarbon@Porphyrin Nanoparticles for Tumor Hypoxia Relief to Enhance Photodynamic Therapy against Liver Metastasis of Colon Cancer. *ACS Nano* **2020**, *14*, 13569.
(34) Dogan, S.; Ince, M.; Sogutlu, F.; Avci, C. B.; Ozel, D.; Yurt, F. Photodynamic Therapy Potential of Cobalt Phthalocyanine in Triple-Negative Breast Cancer. *Polyhedron* **2023**, *245*, No. 116617.
(35) Akin, M.; Saki, N.; Guzel, E.; Orman, B.; Nalbantsoy, A.; Kocak, M. B. Assessment of *in vitro* Cytotoxic, iNOS, Antioxidant and Photodynamic Antimicrobial Activities of Water-soluble Sulfonated Phthalocyanines. *Photochem. Photobiol.* **2022**, *98*, 907−915.
(36) He, Z.; Mei, L.; Connell, M.; Maxwell, C. A. Hyaluronan Mediated Motility Receptor (HMMR) Encodes an Evolutionarily Conserved Homeostasis, Mitosis, and Meiosis Regulator Rather Than a Hyaluronan Receptor. *Cell* **2020**, *9*, 819.
(37) Carvalho, A. M.; Soares da Costa, D.; Paulo, P. M.R.; Reis, R. L.; Pashkuleva, I. Co-Localization and Crosstalk between CD44 and RHAMM Depend on Hyaluronan Presentation. *Acta Biomater.* **2021**, *119*, 114−124.
(38) Wu, M.; Chen, C.; Liu, Z.; Tian, J.; Zhang, W. Regulating the Bacterial Oxygen Microenvironment via a Perfluorocarbon-Conjugated Bacteriochlorin for Enhanced Photodynamic Antibacterial Efficacy. *Acta Biomaterialia* **2022**, *142*, 242.

https://doi.org/10.1021/acs.nanolett.5c00090
Nano Lett. 2025, 25, 4476−4484